14th IEA Heat Pump Conference
15-18 May 2023, Chicago, Illinois

Hybrid thermally driven ionic liquid heat pump water heater and dehumidifer for commercial applications

Rohit Bhagwat[a], Michael Schmid[b], Paul Glanville[c], and Saeed Moghaddam[a*]

[a]University of Florida, 939 Sweetwater Dr, MAE-A Bldg, RM 310, Gainesville, FL, 32611, USA
[b]*Micro Nano Technologies, 747 SW 2nd Ave, Gainesville, FL, 32601, USA*
[c]GTI Energy, 1700 S Mt Prospect Rd, Des Plaines, IL, 60018, USA

Abstract

Water heating and indoor latent cooling loads are great sources of primary energy consumption in many applications. Recently, a semi-open ionic liquid absorption heat pump water heater (AHPWH) has been proposed in which the latent energy in humid air (ventilation, process air, etc.) is used to heat water. This APHWH operates at near ambient pressure, using a novel ionic liquid, enabling stable operation across a wide range of conditions using inexpensive and passive controls eliminating the complexities and costs associated with typical absorption cycles. In this work, we experimentally compare the performance of three configurations of the semi-open heat pump water heater internal heat recovery, at several conditions, including those representative of the standard rating tests as applied to commercial storage-type water heating equipment, to determine their impact on system capacity, coefficient of performance (COP), and water delivery temperature. The results suggest that the impacts varies with the inlet air dewpoint temperature and are substantial at low dewpoints. In hot and humid inlet air conditions, the combined COP reached to 2.55 with a 52 °C water delivery temperature. In these same hot and humid inlet air conditions, the combined COP decreased to 1.93 as the delivery water temperature was increased to 82 °C. These measurements demonstrated the viability of this technology in hot water-intensive applications such as commercial kitchens and food and beverage processing facilities.

Selection and/or peer-review under the responsibility of the organizers of the 14th IEA Heat Pump Conference 2023.

Keywords: Absorption; Ionic Liquid; Heat Pump; Water Heater; Dehumidification; Decarbonization

1. Introduction

With rising energy demand and the dependence on fossil fuels, the world is facing the unprecedented challenges of climate change and energy security [1]. Energy efficiency improvements offer the greatest opportunities for near term decarbonization solutions [2]. Water heating and dehumidification represent two energy intensive processes that have wide-spread application across the industrial and building sector. Several applications such as commercial kitchens and food and beverage processing facilities utilize both processes simultaneously. Recent work has demonstrated the ability of a semi-open absorption heat pump water heater (AHPWH) [3] to harvest the latent energy of air moisture for water heating [4–7]. This AHPWH operates at near ambient pressure, eliminating complexities and costs associated with conventional absorption cycles. A novel ionic liquid (IL) has been successfully implemented enabling the system operation at cycle conditions not possible with conventional salts due to crystallization, and stable operation with inexpensive and passive controls. The system also benefits from compact, light, low-cost plate-and-frame membrane-based heat and mass exchangers [8,9].

Herein, three configurations of the AHPWH system involving different ways of recovering the solution heat leaving the desorber are studied to determine the impacts on system coefficient of performance (COP) and water exit temperature. In the following sections, first, the three system configurations are introduced. Then,

* Corresponding author. *E-mail address:* saeedmog@ufl.edu

details of an experimental setup developed for testing these configurations is discussed. Finally, test results on performance of these systems are compared and the ability of the technology to deliver hot water in commercial applications is analyzed.

2. Experimental system

2.1. System configurations

Previous semi-open AHPWH research has been conducted using the system architecture presented in Figure 1a. In this architecture, heat is added to the process water in the absorber, solution-water heat exchanger (SWHX), and condenser. The use of the SWHX serves to increase the process water temperature, while lowering the desiccant solution temperature prior to its entry into the absorber. A heating oil loop (not shown) is used in all three configurations (Figure 1) to add heat to the desorber. The solution-oil heat exchanger (SOHX) represents the use of flue gas heat to preheat the desiccant solution prior to its entry into the desorber. Figure 1b presents a semi-open AHPWH architecture wherein heat is added to the process water in the absorber and condenser. In this architecture a solution heat exchanger (SHX) is used to recover heat in the solution flow loop, preheating the desiccant solution prior to its entry into the desorber, while cooling the desiccant solution prior to its entry into the absorber. Figure 1c represents a hybrid version of the previous two configurations. In this configuration, heat is added to the process water in the absorber, SWHX, and condenser similar to the configuration shown in Figure 1a. Heat recovery in the desiccant solution flow loop is performed by the SHX in a similar fashion as the configuration shown in Figure 1b. The addition of the SWHX in this configuration is intended to lower solution desiccant temperature entering the absorber to increase the system's latent capacity. In this paper, the experimental performance of these configurations is compared.

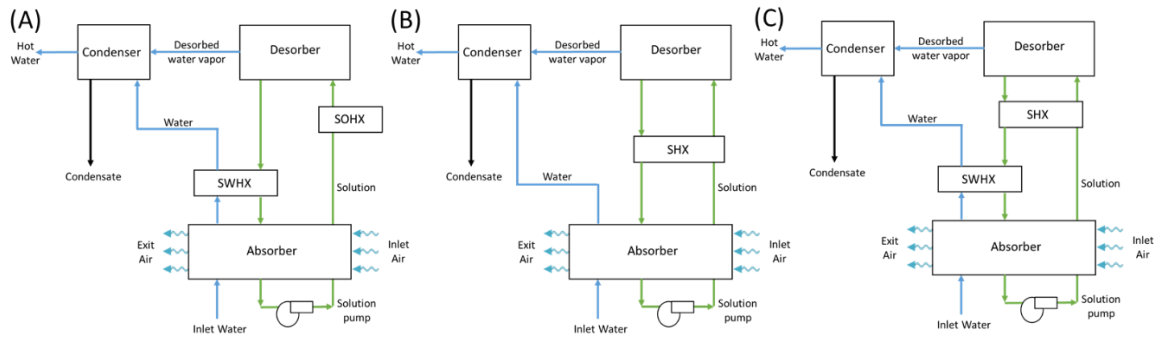

Figure 1. The semi-open absorption heat pump water heater system configuration schematics using solution-water and solution-oil heat exchangers (A), solution heat exchanger (B), and solution-water and solution heat exchangers (C).

2.2. Instrumentation Diagram

A single-effect liquid desiccant AHPWH was fabricated and integrated into a test suite (Figure 2). Two configurations of this AHPWH system (Figure 1b and 1c) were tested in this study. This experimental data was compared with legacy data for the AHPWH operating in the configuration shown in Figure 1a [4,6,7]. In each configuration, the system operates in a cycle in which water vapor is absorbed from the air flow in the absorber and is subsequently liberated in the desorber (via heating) with the heat of absorption, condensation, and recovery being used to heat the process water. Within the absorber, the concentrated desiccant solution flows down the absorber plate while interfacing with the air flow through the membrane. The water vapor is absorbed by the solution. The dilute (i.e., water-rich) solution then exits the absorber and is pumped to the desorber where it is regenerated. Depending on the system configuration, one or more heat exchangers are used to recover energy of the solution exiting the desorber to either heat the desorber inlet solution and/or the process water.

The experimental test setup consists of three primary flow loops including the solution, water, and air flow loops as well as two secondary flow loops: the heating oil loop and the air flow loop (cf. Figure 2). The IL solution exiting the absorber is pumped to the desorber by a small variable speed gear pump. The absorber is located within the closed air loop (cf. Figure 2). A chiller is used in the process water loop to control the inlet temperature and water flow rate to the system absorber, condenser, and heat exchangers (as applicable). To control the humidity level within the air loop, a steam generator in conjunction with a custom-made steam distribution manifold are utilized. To control the air temperature, a secondary water loop is connected to a

heating/cooling coil installed within the air duct. A variable speed axial fan is used to circulate air through the air loop. The heating oil loop, which powers the desorber, utilizes a heating oil bath and synthetic oil SIL 180.

The solution and water flow rates are measured using positive displacement and turbine flow meters, respectively. Due to the elevated temperature of the oil flow loop, a high-temperature positive displacement flow meter is used to measure the oil flow rate. The air flow rate is measured using a pitot tube sensing element mounted within the air loop duct. Multiple sensing ports along the length of the sensing element are used, and internally averaged to ensure accurate air flow rate measurement. All liquid temperatures were measured using T-type thermocouples. The process air temperature and relative humidity are measured using thin-film capacitive sensors. The absorber solution inlet and outlet concentrations are measured using two inline refractive index (RI) sensors. RI instead of Coriolis effect is used because the variation in density for ILs is insignificant over a wide concentration range, making accurate measurement of the concentration infeasible. Curve fits have been developed to establish RI values as a function of IL concentration and temperature. The primary system temperature, flow rate, RI, and air velocity are recorded using a data acquisition system. A second data acquisition system is used to record the air temperature and relative humidity. Time stamps are used to combine the data collected by each data acquisition system to enable a system level data analysis.

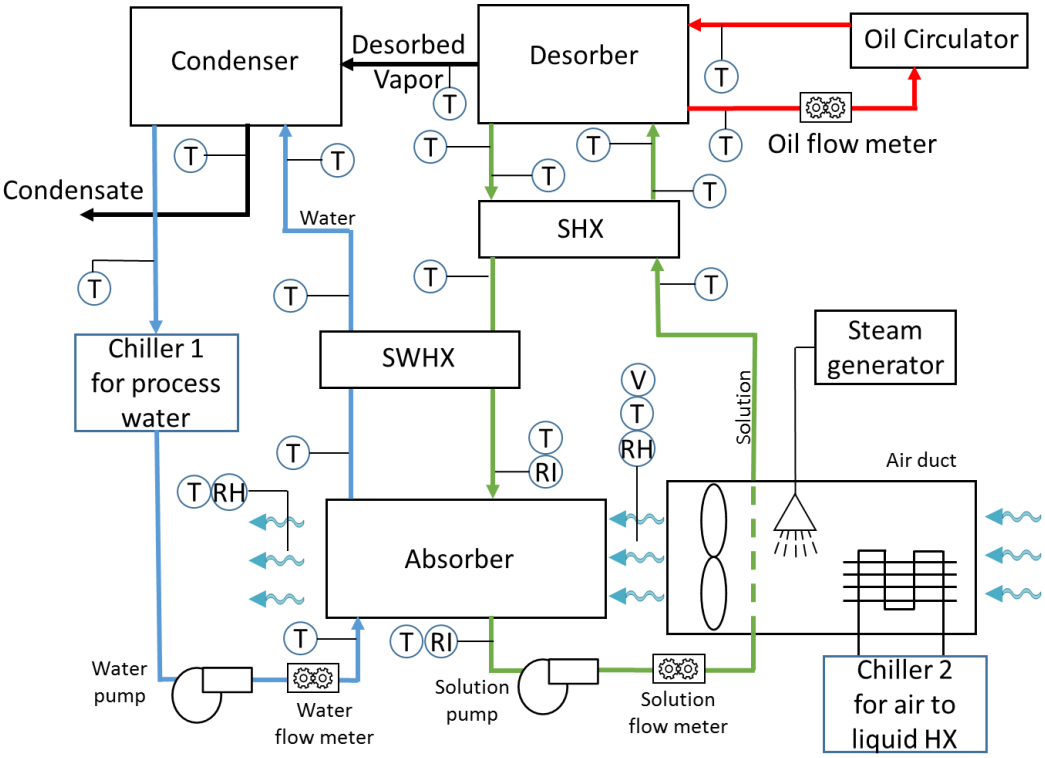

Figure 2. Instrumentation diagram of the experimental test system, when testing the system configuration shown in Figure 1c.

2.3. Absorber

A new generation absorber is utilized in this study. Comparison of this absorber with the configurations of absorbers used in our previous studies are presented in Table 1. The overall absorber configuration has remained the same between different generations. A schematic of an absorber panel showing the desiccant solution, cooling water, and air flows is shown in Figure 3. The absorber used in this study is fabricated from acrylonitrile butadiene styrene (ABS) sheets. Each absorber plate has an internal cooling water core containing water channels and distribution manifolds. The desiccant solution flows on the two outer surfaces of each plate. The plate surfaces are machined to include features designed to slow and spread the solution flow to "wet" the entire surface (front and back) of each panel [8,9]. A membrane is then bonded over the surface features to constrain the solution. Lastly, manifolds are bonded on the top and bottom of each side of the ABS sheet-membrane assembly (i.e., a panel) to direct the IL flow through the gap formed in between the ABS surface and membrane, and the water to the internal water cavity. Air flows across the panels (cf. Figure 3) through 3 mm gaps formed in between them within the absorber assembly.

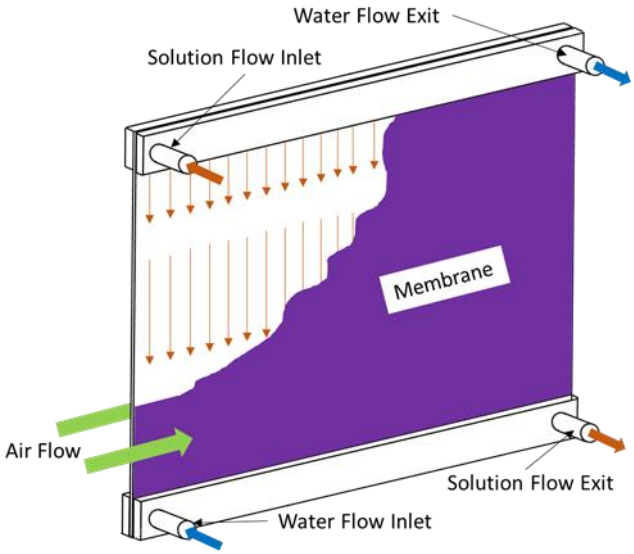

Figure 3. A schematic of a single absorber plate showing that air flows across the membrane while exchanging moisture with the desiccant solution constrained behind the membrane.

Table 1: Absorber design properties and parameters.

Absorber	Gen 1[4]	Gen2[5]	Gen 3[6]	This study
Number of panels	4	7	13	14
Active surface area (m^2)	0.42	0.92	1.89	3.30
Active plate volume (m^3)	0.0084	0.008	0.01191	0.0091
Active surface area/volume ratio (m^{-1})	50	115	158.59	363.6
Plate material	Metal & 3D printed polymer	Polycarbonate	Polycarbonate	ABS
Plate construction	CNC Machined, Adhesive bonded	CNC Machined; Thermal & Adhesive bonded	CNC Machined; Thermal & Adhesive bonded	CNC Machined; Thermal & Adhesive bonded
Solution side fin height	1.5 mm	1mm	0.6 mm	0.6 mm
Membrane constraint	Not bonded on the fins	Thermally bonded on fins	Thermally bonded on fins	Thermally bonded on fins
Membrane pore size	1 µm	1 µm	1 µm	1 µm

2.4. Desorber and Condenser

In contrast to the absorber, the desorber design has remained the same in all our studies. In the desorber, the dilute solution is supplied to the desorber surface by a distribution manifold located at the top of the desorber surface (Figure 4). To ensure a uniform distribution of the solution over the desorber surface (Figure 4A) and to enhance the desorption rate, surface structures described in our earlier studies are utilized here [10]. The desorber surface is heated using silicone oil in a counter flow heat exchange configuration (Figure 4A). To utilize the heat of the desorbed vapor, a condensing surface is built adjacent to the desorber surface, separated by a porous polytetrafluoroethylene (PTFE) membrane (Figure 4B). A critical function of this membrane is to eliminate IL carryover from the desorber while permitting water vapor migration to the condensing surface. The condensing surface is used as the final heating stage of the process water within the AHPWH.

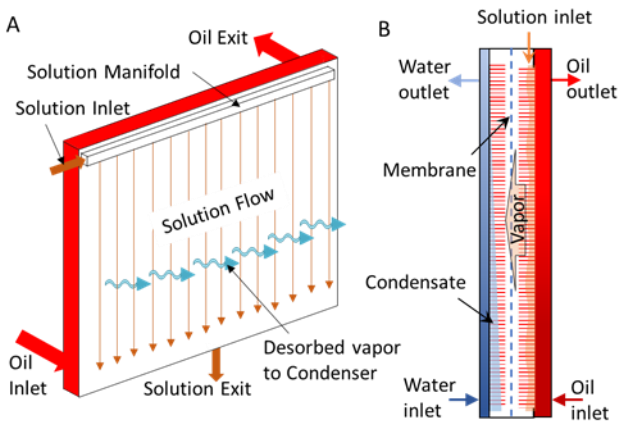

Figure 4. A schematic of the desorber and condenser assembly showing solution falling film flow configuration (A) and the desorption of water vapor, its flow through a PTFE membrane, and subsequent condensation and heating of the process water in the condenser (B).

2.5. Data reduction and uncertainty analysis

The system performance presented in the results and discussion section is calculated based on the measured data described above. The system latent capacity is calculated using Eq. (1).

$$Q_{latent} = \dot{V}_{air}\, \rho_{air}\, h_{fg}\, (\omega_{air\_in} - \omega_{air\_out}) \tag{1}$$

where $\dot{V}_{air}$ is the absorber air flow rate; ω_{air_in} and ω_{air_out} are the absorber air inlet and exit absolute humidity, respectively; ρ_{air} is the air density as calculated from standard tables using the measured air inlet conditions; and h_{fg} is the water latent heat of evaporation. The desorber heat input is calculated using Eq. (2).

$$Q_{oil} = \dot{V}_{oil}\, \rho_{oil}\, c_{p\_oil} (T_{des\_oil\_in} - T_{des\_oil\_out}) \tag{2}$$

where $\dot{V}_{oil}$ is the desorber oil flow rate; $T_{des\_oil\_in}$ and $T_{des\_oil\_out}$ are the desorber oil inlet and outlet temperatures, respectively; ρ_{oil} is the oil density; and c_{p_oil} is the oil thermal capacity calculated using curve fits derived from data provided by Clearco for their SIL 180 silicone oil. The system water heating capacity is calculated using Eq (3).

$$Q_{water} = \dot{V}_{water}\, \rho_{water}\, c_{p\_water} (T_{water,cond\_out} - T_{water,abs\_in}) \tag{3}$$

where $\dot{V}_{water}$ is the process water flow rate; $T_{water,\ cond\_out}$ and $T_{water,\ abs\_out}$ are the condenser water outlet and absorber water inlet temperatures, respectively; ρ_{water} is the water density; and c_{p_water} is the water thermal capacity. The system latent heat capacity along with the desorber heat input are used in Eq. (4) to calculate the system dehumidification COP.

$$COP_{dehumidification} = \frac{Q_{latent}}{Q_{oil}} \tag{4}$$

The system water heating capacity along with the desorber heat input are used in Eq. (5) to calculate the system heating COP.

$$COP_{heating} = \frac{Q_{water}}{Q_{oil}} \tag{5}$$

The combined system COP is the addition of the system water heating and system dehumidification COPs as shown in Eq. (6).

$$COP_{combined} = COP_{heating} + COP_{dehumidification} \tag{6}$$

The uncertainty was calculated using an engineering equation solver (EES) uncertainty propagation subroutine. The subroutine is based on NIST guidelines[11] and assuming that the individual measurements are uncorrelated and random, the uncertainty in the calculated quantity can be estimated using Eq. (7).

$$U_Y = \sqrt{\sum_i \left[\frac{\partial Y}{\partial X}\right]^2 U_{X_i}^2} \tag{7}$$

Table 2 below lists all the relevant measurement errors and uncertainties in this experimental study.

Table 2. Measurement error and uncertainty propagation.

Variable	Uncertainty
Fluid temperatures -All T-type TC	±0.8°C
Solution volumetric flow rate	±0.25% reading
Solution RI	±0.5% scale range (0.0003nD)
Water volumetric flow rate	±1% full scale (0.5 LPM)
Air volumetric flow rate	±2% reading
Oil volumetric flow rate	±0.5% reading
Air temperature	±0.3% reading
Air relative humidity	±1.8% RH
Oil heat	±3.7%
Water heat	±2.0%
Concentration (X%)	±0.15%
COP	±4.2%

2.6. Test Conditions

Each configuration was tested at the inlet air and water conditions listed in Table 3. The first test condition represents the inlet water and air temperatures outlined in the Electronic Code of Federal Regulations (e-CFR) to establish water heating Uniform Energy Factor (UEF) performance[12]. The inlet air, IL solution, and oil flow rates as well as the oil inlet temperature have been held constant at 155 cfm, 300 mlpm, 2.85 lpm, and 148 °C, respectively.

Table 3. System inlet air and water test conditions.

Test Condition	Inlet Air Conditions			Water Inlet Conditions	Notes
	Dry Bulb Temp [°C]	Dew Point Temp [°C]	Rel Hum [%]	Temp [°C]	
1	19.7	8.99	50.00	14.4	UEF Conditions
2	19.7	8.99	50.00	30.0	
3	26.8	24.1	85.00	15.0	
4	26.8	24.1	85.00	30.0	
5	30.0	23.9	70.00	15.0	
6	30.0	23.9	70.00	30.0	
7	21.3	13.2	60.00	15.0	
8	21.3	13.2	60.00	30.0	
9	35.0	33.1	90.00	15.0	
10	35.0	33.1	90.00	30.0	

3. Results

Legacy data is presented herein to compare the performance of system configuration A (cf. Figure 1) to configurations B and C [4–7]. The system performance data presented for configurations b and c has been collected as part of this experimental study.

3.1. Configuration B

As shown in Figure 5 for configuration B (cf. Figure 1b), the system water heating capacity depends on both the air and water inlet conditions. As expected, the system water heating capacity increases as the inlet air dewpoint increases. This is due to the increase in the air temperature and moisture content with increasing dewpoint temperature, meaning that more energy is available in the air (more humidity). Also, the water heating capacity decreases as the inlet water temperature increases, because increasing the water temperature elevates the solution temperature resulting in reduction in the heat added to the water.

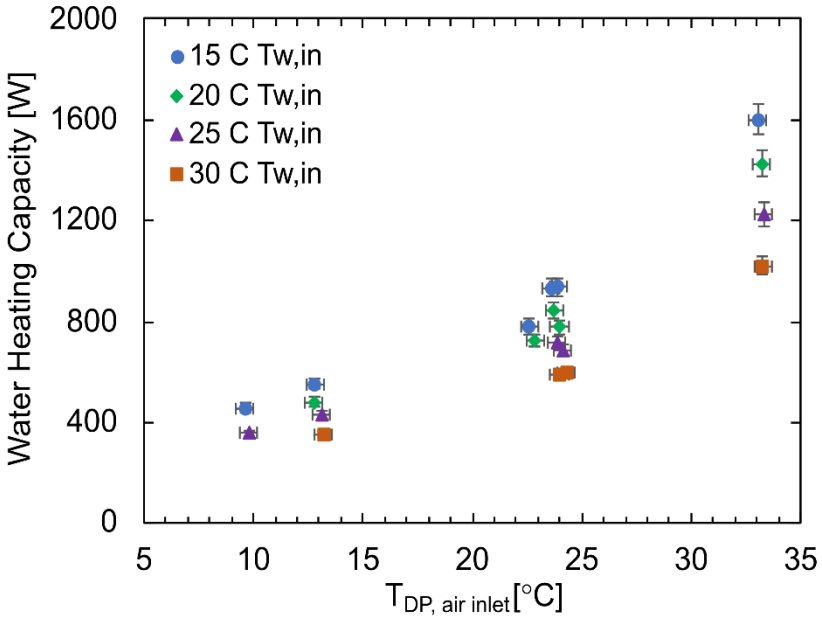

Figure 5. System water heating capacity as function of air inlet dew point temperature and water inlet temperature (Tw, in) when operating in configuration B. The inlet air, IL solution, and oil flow rates as well as the oil inlet temperature have been held constant at 155 cfm, 300 mlpm, 2.85 lpm, and 148 °C, respectively.

Similarly, as the system water heating capacity increases as a function of the increasing inlet air dewpoint temperature and decreasing water temperature, the system heating COP (Figure 6a) and dehumidification COP (Figure 6b) also show similar trends. The very low dehumidification COP at low inlet air dewpoint temperatures is a result of the relatively high absorber solution inlet temperatures (~ 40 °C). While these temperatures served to heat the water in the absorber, they limit the amount of latent heat removed from the air, lowering the system dehumidification COP.

3.2. Configuration C

Similar to configuration A (cf. Figure 1a), configuration C (cf. Figure 1c) uses heat recovery from the solution flow loop for process water heating. However, in configuration C, the solution inlet temperature to SWHX used for heat recovery is substantially lower than that in configuration A, as the solution flow has already been used for heat recovery in the SHX. The water heating capacity, and heating and dehumidification COPs trends for configuration C (cf. Figure 1c) are consistent with those exhibited in configuration B (Figure 7). At a given inlet water temperature, the water heating capacity and heating and dehumidification COPs all increase with increase inlet air dewpoint temperature. As discussed in the section above, this is due to the increase in the energy available in the inlet air as its dewpoint temperature is increased. Although not shown in Figure 7, similar to the trend in configuration B the system capacity and performance decreases with increasing absorber water inlet temperature.

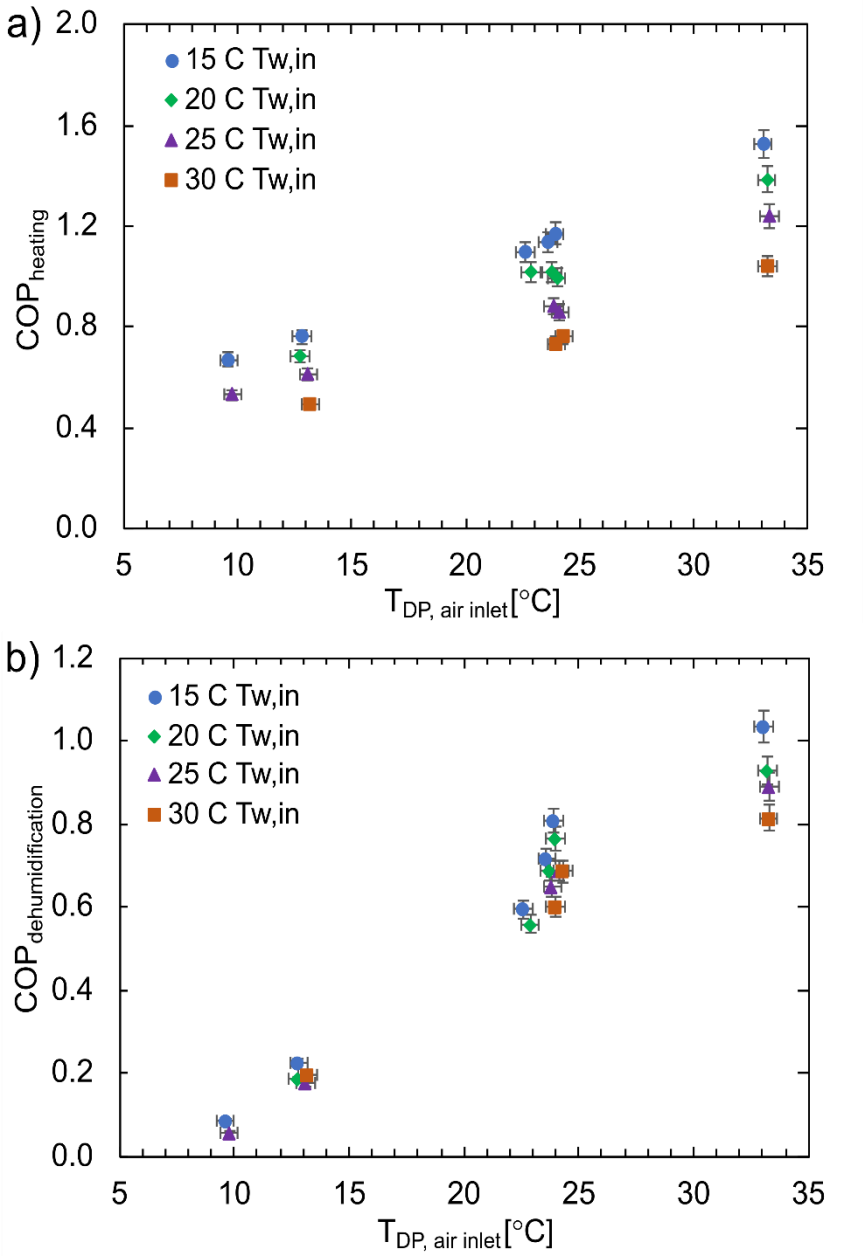

Figure 6. System heating (a) and dehumidification (b) COP as a function of air inlet dew point temperature and water inlet temperature (Tw,in) when operating in configuration B. The inlet air, IL solution, and oil flow rates as well as the oil inlet temperature have been held constant at 155 cfm, 300 mlpm, 2.85 lpm, and 148 °C, respectively.

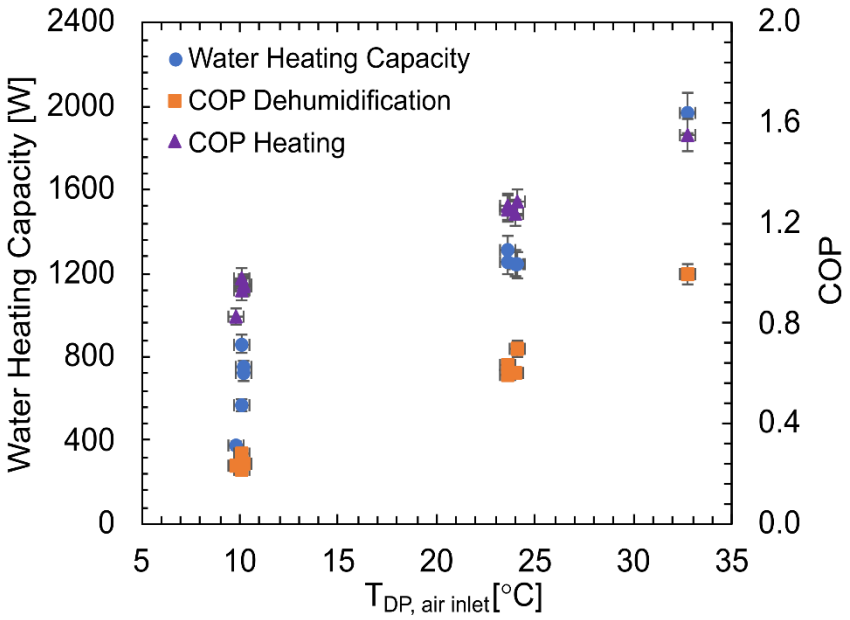

Figure 7. System water heating capacity as function of air inlet dew point temperature when operating in Configuration C. The inlet air, IL solution, and oil flow rates as well as the oil and water inlet temperature have been held constant at 155 cfm, 300 mlpm, 2.85 lpm, 148 °C, and 15 °C respectively.

3.3. Comparison between Different System Configurations

As shown in Figure 8, the differences in the solution heat recovery process as defined by Configurations A, B, and C impact the system water heating capacity. As is shown in Figure 8, the addition of the SWHX in the solution loop (Configuration C) provides a fairly constant increase in system water heating capacity relative to Configuration B over a wide range of inlet air dewpoint temperature. The legacy water heating capacity data for Configuration A, does not demonstrate the same increasing capacity with increasing inlet air dewpoint temperatures [5].

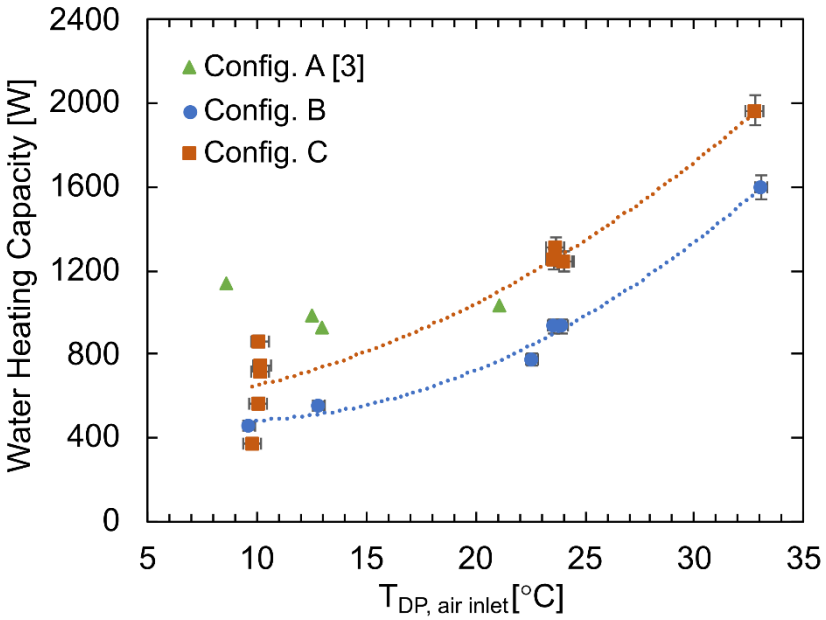

Figure 8. System water heating capacity as a function of air inlet dew point temperature for all three configurations. The inlet air, IL solution, and oil flow rates as well as the oil and water inlet temperatures have been held constant at 155 cfm, 300 mlpm, 2.85 lpm, 148 °C, and 15 °C, respectively.

As shown in Figure 9, the addition of the SWHX has increased both the heating and dehumidification COPs in at low inlet air dewpoints when compared to the COPs of configuration B (Figure 6). However, as

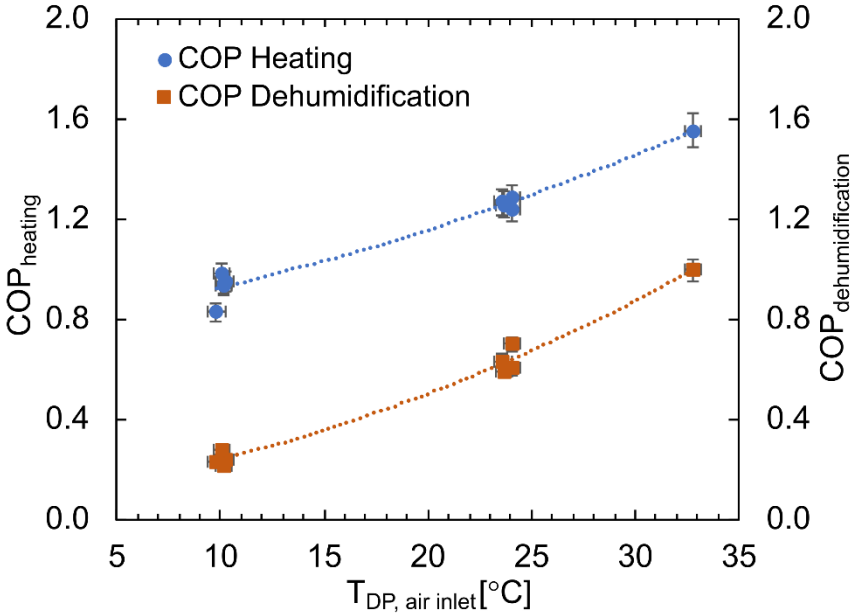

Figure 9. System heating and dehumidification COP as a function of air inlet dew point temperature for configuration C. The inlet air, IL solution, and oil flow rates as well as the oil and water inlet temperatures have been held constant at 155 cfm, 300 mlpm, 2.85 lpm, 148 °C, and 15 °C, respectively.

can be seen in Figure 10 this improved COP of configuration C as compared to configuration B at low inlet air dewpoint temperatures, becomes smaller as the inlet air dewpoint increases. In comparison the combined COP of configuration A, is the best at low inlet air dewpoint temperatures, with its performance being relatively flat as the inlet air dewpoint is increased. This demonstrates the configuration C, provides the best performance

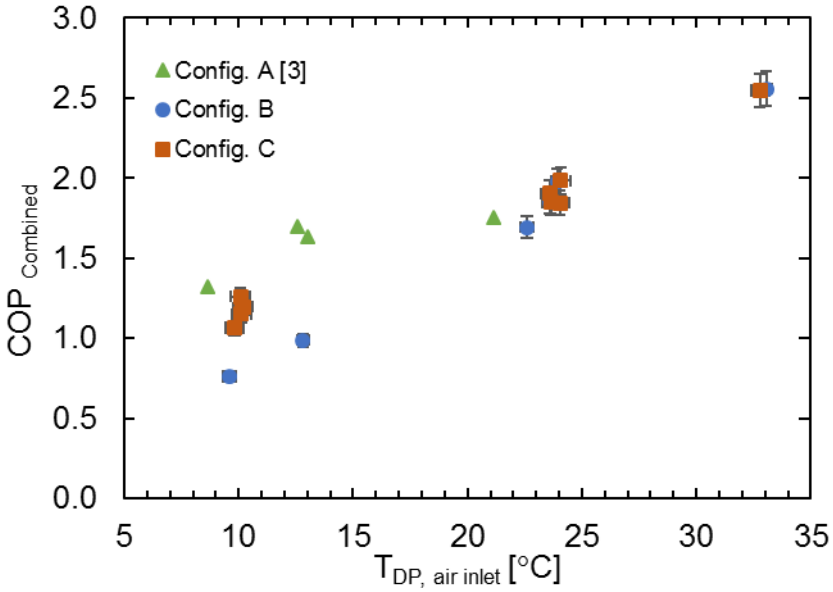

Figure 10. Combined system COP as a function of air inlet dew point temperature for all three configurations. The inlet air, IL solution, and oil flow rates as well as the oil and water inlet temperatures have been held constant at 155 cfm, 300 mlpm, 2.85 lpm, 148 °C, and 15 °C, respectively.

across a wide range of inlet air conditions. At low inlet air dewpoint conditions, the performance of configuration A and C are comparable, but better than that of configuration B. At high inlet dewpoint conditions, the performance of configuration B and C are comparable, but better than that of configuration A.

3.4. Delivery water temperature

For residential water heating applications, the UEF test conditions dictate a water delivery temperature of 51.7 °C. In legacy research, the water delivery rate was held constant, and the water delivery temperature was allowed to fluctuate based on the inlet air and water conditions[5]. In this study, for configurations B and C, the delivery water temperature was maintained at ~ 52 °C, and the water delivery rate was varied based on the inlet air and water conditions. As the performance of this AHPWH improves with increasing air inlet temperature and humidity, a potential application is commercial water heating for kitchens using the kitchen latent load.

The commercial water delivery temperature is 82.2 °C. As such, the ability of the system to deliver water at this temperature, at hot and humid air inlet temperatures, and the impact on system performance was investigated. At an inlet air dewpoint temperature of 32.7 °C and an inlet water temperature of 15 °C, the heating COP of the system decreases from 1.55 to 1.07 as the water delivery temperature is increased from 52 °C to 82 °C for the system operating in Configuration C. Under this same conditions and configuration, the dehumidification COP decreases slightly from 0.99 to 0.86. The decrease in heating COP is expected as the condenser operating temperature has been increased, while the desorber oil inlet temperature has been held constant. Future studies are warranted to increase the system COP by changing its regeneration temperature as well as IL properties.

4. Conclusions

A lab scale IL absorption heat pump water heater system was experimentally tested in two configurations, across a range of inlet air and water conditions, including those delineated for UEF testing. The system performance of these two configurations were compared to each other, as well as, a third configuration used in previous research efforts. These configurations demonstrated the ability to deliver 52 °C water at UEF conditions at a heating COP of 1.26 [6] (configuration A), 0.67 (configuration b), and 0.98 (configuration C). This performance increased to a heating COP of 1.52 (configuration B) and 1.55 (configuration C) at an inlet air dewpoint of ~ 32 °C. These COPs compare well to the primary COP of 1.42 [13] of the most efficient electric HPWH (UEF = 4.07) on the market today.[14] Additionally, the ability to deliver 82 °C water at hot and humid inlet air conditions demonstrated the viability of this technology in commercial water heating applications. The use of IL demonstrated the robustness of the system in providing water heating across a wide operational range, without control equipment for mitigating crystallization. Further optimization of the system flow rates offers the ability to improve.

Nomenclature

ABS	acrylonitrile butadiene styrene
AHPWH	absorption heat pump water heater
CFM	cubic feet per minute
COP	coefficient of performance
$COP_{combined}$	sum of $COP_{heating}$ and $COP_{dehumidification}$
$COP_{dehumidification}$	dehumidification capacity (latent cooling)/thermal energy consumed
$COP_{heating}$	water heating capacity/thermal energy consumed
e-CFR	electronic code of federal regulations
HX	heat exchanger
IL	ionic liquid
LPM	liters per minute
GHG	greenhouse gas
mLPM	milliliters per minute
PTFE	polytetrafluoroethylene
RI	refractive index
RH	relative humidity
SHX	solution heat exchanger
SOHX	solution-oil heat exchanger
SWHX	solution-water heat exchanger
$\dot{m}$	mass flow rate (kg/sec)

T	temperature (°C)
Tw,in	water inlet temperature (°C)
$T_{DP,in}$	inlet air dew point temperature (°C)
UEF	uniform energy factor

Acknowledgements

This work was sponsored by the U. S. Department of Energy, Office of Energy Efficiency and Renewable Energy (EERE), under Award Number DE-EE0009162 with the University of Florida. The authors would also like to acknowledge Mr. Antonio Bouza, Ms. Coriana Fitz, and Dr. Isaac Mahderekal from the U.S. DOE Building Technologies Office (BTO) for their support of this research.

References

[1] Jarraud M, Steiner A. Summary for policymakers. vol. 9781107025. 2012. https://doi.org/10.1017/CBO9781139177245.003.
[2] Cresko J. Industrial Decarbonization Roadmap 2022.
[3] Moghaddam S, Chugh D, Nasrisfahani R, Bigham S, Fazeli SA, Yu D, et al. Open absorption cycle for combined dehumidification, water heating, and evaporative cooling, 2018.
[4] Chugh D, Gluesenkamp K, Abdelaziz O, Moghaddam S. Ionic liquid-based hybrid absorption cycle for water heating, dehumidification, and cooling. Appl Energy 2017;202:746–54. https://doi.org/10.1016/j.apenergy.2017.05.161.
[5] Chugh D, Gluesenkamp KR, Abu-Heiba A, Alipanah M, Fazeli A, Rode R, et al. Experimental evaluation of a semi-open membrane-based absorption heat pump system utilizing ionic liquids. Appl Energy 2019;239:919–27. https://doi.org/10.1016/j.apenergy.2019.01.251.
[6] Gluesenkamp KR, Kumar N, Abu-heiba A, Patel V. Semi-open absorption water heater : experimental results 2020:1–11.
[7] Gluesenkamp KR, Chugh D, Abdelaziz O, Moghaddam S. Efficiency analysis of semi-open sorption heat pump systems. Renew Energy 2016:1–10. https://doi.org/10.1016/j.renene.2016.07.075.
[8] Mortazavi M, Isfahani Nasr R, Bigham S, Moghaddam S. Absorption characteristics of falling film LiBr (lithium bromide) solution over a finned structure. Energy 2015;87:270–8.
[9] Nasr Isfahani R, Bigham S, Mortazavi M, Wei X, Moghaddam S. Impact of micromixing on performance of a membrane-based absorber. Energy 2015. https://doi.org/10.1016/j.energy.2015.08.006.
[10] Mortazavi M, Schmid M, Moghaddam S. Compact and efficient generator for low grade solar and waste heat driven absorption systems. Appl Energy 2017;198:173–9. https://doi.org/10.1016/j.apenergy.2017.04.054.
[11] Taylor BN, Kuyatt CE. Guidelines for Evaluating and Expressing the Uncertainty of NIST Measurement Results. Technology (Singap World Sci) 1994:2.
[12] Subpt B, App E. Pt. 430, Subpt. B, App. E 2016.
[13] April U. DNV GL - ENERGY DEER Water Heater Calculator Documentation 2022.
[14] ENERGY STAR Certified New Homes : ENERGY STAR n.d.